Fall Technical Meeting
of the Western States Section of the Combustion Institute
Hosted by the University of California, Irvine
Oct 25-27, 2009

# A shock tube study on the pyrolysis of 1,4-dioxane

*X. Yang[1], A. W. Jasper[2], B. R. Giri[1,4], J. H. Kiefer[3] and R. S. Tranter[1*]*

[1] *Chemical Sciences and Engineering Division, Argonne National Laboratory, 9700 S. Cass Avenue, Argonne, IL-60439.*

[2] *Combustion Research Facility, Sandia National Laboratory, P.O. Box 969, Livermore, CA-94551*

[3] *Department of Chemical Engineering, 810 S. Clinton St., University of Illinois at Chicago, Chicago, IL-60607*

[4]*Current Address: Alberta Sulphur Research Ltd, 3535 Research Road NW, Calgary, Alberta T2L 2K8, Canada*

The dissociation of 2% 1,4-dioxane dilute in krypton was studied in a shock tube, ST, using laser schlieren densitometry, LS, at 1550-2100 K and 123±2 Torr. Products were identified by ST/time-of-flight mass spectrometry. 1,4-dioxane was found to initially dissociate via C-O bond fission followed by a 2,6 H-atom transfer to the O atom at the scission site. Simulations of the LS profiles with a 72 reaction mechanism gave excellent agreement. Rate coefficients for the initial dissociation yielded $k_{1,123Torr}(T) = (2.10 \pm 0.30) \times 10^8 \times \exp(-15006/T)$ $s^{-1}$. Optimization of the simulations yielded $k_{37} = (2.25 \pm 0.60) \times 10^3 \times T^3 \times \exp(860/T)$ $cm^3mol^{-1}s^{-1}$ for H-abstraction from 1,4-dioxane by OH radicals.

## 1. Introduction

Fuels derived from tar sands and oil shales contain a higher proportion of cyclic species than those derived from more conventional feedstocks and interest in the combustion mechanisms of these species is growing. One class of compounds that is of particular interest is the cyclic ethers which may be formed as intermediates in the combustion of non-traditional fuels. The literature concerning the kinetics and mechanisms of the pyrolysis and oxidation of cyclic ethers is sparse and thus we have started to investigate the pyrolysis of saturated cyclic ethers at high temperatures in a shock tube. Cyclohexane (zero O-atoms) can be considered as the first species of the series of saturated six-member rings that extends through pyran (one O-atom), 1,3- and 1,4- dioxane (two O-atoms) to 1,3,5-trioxane (three O-atoms). At the extremes of this series two distinct dissociation mechanisms operate. 1,3,5-Trioxane dissociates via a concerted mechanism to give three formaldehyde molecules [1] whereas a recent shock tube (ST) / laser schlieren densitometry (LS) study of cyclohexane pyrolysis [2] demonstrated that cyclohexane dissociates via isomerization to 1-hexene followed by dissociation of 1-hexene.

The current work focuses on the dissociation of 1,4-dioxane which has been previously studied at low temperatures by Kuchler and Lambert [3] and Battin et al. [4]. Both studies concluded that the dissociation of 1,4-dioxane occurred via a free radical mechanism. Battin et al. proposed the following mechanism where the initial step is scission of a C-C bond followed by dissociation of the

* Corresponding author: tranter@anl.gov

linear radical to formaldehyde and ethane, reaction (II). They suggested that homolysis of formaldehyde via reaction (III) would then initiate the chain reaction. However, at the temperatures and pressures of their study (33 Torr, 783 and 825 K) this later step seems unlikely to occur homogeneously in the gas phase due to the thermal stability of formaldehyde [1,5].

$$C_4H_8O_2 \rightarrow CH_2OCH_2CH_2OCH_2 \quad \text{(I)}$$
$$CH_2OCH_2CH_2OCH_2 \rightarrow CH_2O + CH_2O + C_2H_4 \quad \text{(II)}$$
$$CH_2O \rightarrow H + HCO \quad \text{(III)}$$
$$H + C_4H_8O_2 \rightarrow C_4H_7O_2 + H_2 \quad \text{(IV)}$$
$$C_4H_7O_2 \rightarrow CH_2O + HCO + C_2H_4 \quad \text{(V)}$$

The mechanism and kinetics of the pyrolysis of 1,4-dioxane have thus been investigated at elevated temperatures by ST/LS and ST/TOF-MS (time-of-flight mass spectrometry) experiments. These studies yield direct measurements of the initial rate of dissociation of 1,4-dioxane and the identities of products which guide development of a mechanism for the pyrolysis of 1,4-dioxane. In 1,4-dioxane scission can potentially occur at both C-C and C-O bonds leading to a complex distribution of products. Furthermore, if 1,4-dioxane were to dissociate via a concerted mechanism similar to 1,3,5-trioxane then this could lead directly to the products of reaction (II). To investigate the initial dissociation of 1,4-dioxane a complementary theoretical investigation was conducted and the theoretical results guided the development of a pyrolysis mechanism for 1,4-dioxane. The results of the experimental and theoretical studies are presented in this paper along with the development of a mechanism for pyrolysis of 1,4-dioxane.

## 2. Experimental

The LS and TOF-MS experiments were performed in a diaphragmless shock tube, DFST, which has been fully described elsewhere [6]. The driver section of the DFST contains a fast acting valve which replaces the more traditional diaphragm. When the valve is closed the driver and driven sections can be filled to the desired loading pressures and the DFST is fired by rapidly opening the valve. By varying both the driver section pressure, $P_4$, and the driven section pressure, $P_1$, the pressure behind the incident and reflected shock waves, $P_2$ and $P_5$ respectively, can be constrained to very narrow ranges, typically < ±3%, over a wide range of temperatures [6].

**DFST/LS**: The laser schlieren technique utilizes deflection of a narrow beam from a He/Ne laser to measure density gradients behind the incident shock wave. The technique has been fully described previously, [7,8] and a schematic of the laser schlieren apparatus is shown in Fig. 1(a). The driven section of the shock tube has an internal diameter of 7.01 cm and the quartz windows, through which the laser beam passes are located sufficiently far downstream to allow the shock wave to be fully developed after firing the DFST. A set of six pressure transducers evenly spaced along the side of the driven section are centered around the LS windows, and incident shock wave velocities were obtained by interpolation of time intervals taken for the shock wave to pass between successive transducers. From these velocities and the loading conditions the temperature and pressure behind the incident shock wave are calculated assuming frozen conditions. The uncertainty in velocity is estimated as 0.2%, corresponding to a temperature error of less than 0.5%, here amounting to the order of 10-15K. The molar refractivity of Kr = 6.367 [9], while that of 1,4-dioxane, 21.65, was calculated from its refractive index and molar density. The normal assumption was made that the mixture molar refractivity does not vary with extent of reaction.

Examples of the raw signal from two LS experiments are shown in Fig. 2. In both Figs. 2a and b the large positive spike and preceding negative signal are due to passage of the shock front through the laser beam [8]. The flat signal prior to arrival of the incident shock wave in the observation zone is used to establish a baseline in each experiment. The sharp excursion in the signal on the right hand side of the positive spike represents signal due to chemical reaction, Fig. 2a. While for the higher temperature and pressure experiments, the dissociation is so rapid that the break in the signal is much harder to identify, Fig. 2b. However, it is usually easier to identify the break on a semi-log plot of density gradients that are derived from the raw data such as those shown in Figs. 3a and b which correspond to Figs. 2a and b respectively. Figs. 2b and 3b show a minimum that dips below the baseline before recovering Such minima are characteristic of net exothermic processes. The shape of the profile and location of the transition from net positive to negative density gradients are valuable targets for model development.

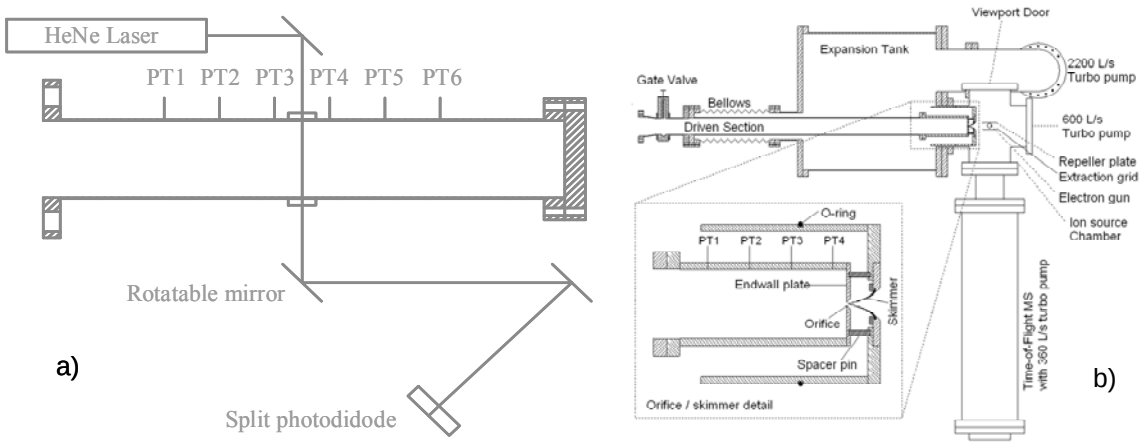


**Figure 1**: (a) Schematic of the LS apparatus. The rotating mirror is used to sweep the laser beam across the detector at a known rate permitting the detector response to be calibrated before each experiment. (b) Schematic of the TOF-MS interface. The inset shows the end of the shock tube and the nozzle/skimmer arrangement in detail**.**

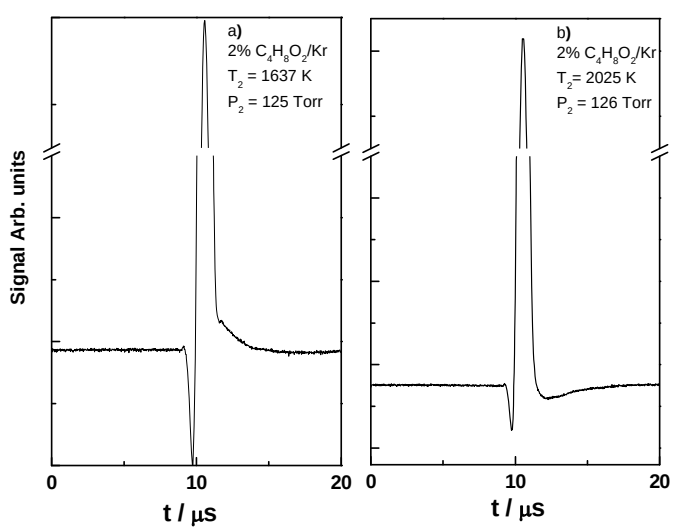


**Figure 2**: Laser schlieren profiles showing dissociation in 2% $C_4H_8IO_2$ / Kr mixtures. The positive spike and preceding valley are due to shock front/laser beam interaction

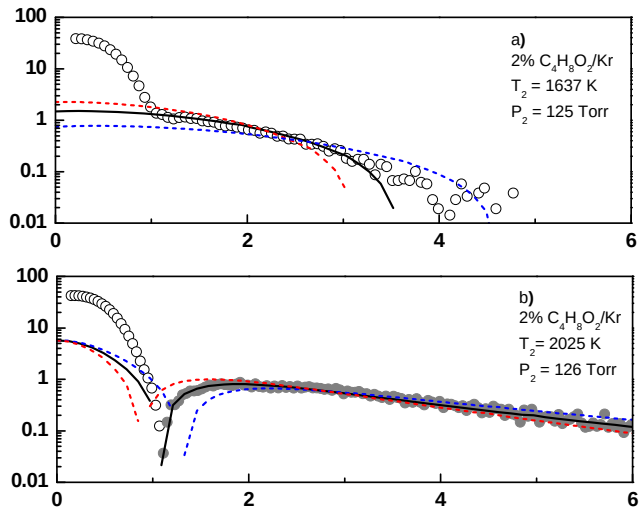


**Figure 3:** Plots of density gradients derived from laser schlieren experiments. a) and b) correspond to the raw signals shown in Fig. 2a and b respectively. Points represent experimental data and absolute values are plotted. Open symbols represent positive values while closed symbols represent negative values. The solid black lines in both figures are simulation results obtained with the model in Table II. The effects of varying $k_1$ and $k_{37}$ are shown in panels a) and b) respectively: a) Red line: $k_1$*1.5; Blue line $k_1$*0.5. b) Red line $k_{37}$*2; Blue line $k_{37}$*0.5

**DFST/TOF-MS:** The interface between the DFST and TOF-MS is shown in Fig. 1(b) and has been described in detail elsewhere [10]. In contrast to the DFST/LS technique where measurements are made behind the incident shock wave, the ST/TOF-MS method is used to study reactions behind the reflected shock wave. Gases continually flow through an orifice centered in the endwall of the driven section of the shock tube. This orifice forms the first stage of a differentially pumped molecular beam sampling system that quenches the gases eluting from the shock tube and introduces them into the ion source of the TOF-MS [10].

Ions are created by electron impact ionization, 30eV, and ion packets are injected into the flight tube of the TOF-MS at 25 μs intervals, 40 kHz. This sampling frequency is really too low to provide accurate kinetic data but it does yield clean, well defined mass spectra from which species can be identified. Examples of the pre-shock and post shock mass spectra from one experiment are shown in Fig. 4. The pre-shock mass spectrum, Fig. 3a, is consistent with the 70 eV literature mass spectrum of 1,4-dioxane [11] although the lower ionization energies used here create somewhat less fragmentation and the very minor peaks in the literature MS at m/z=17 and 18 are not seen at all in Fig. 4a. This could either be because they are not generated at 30 eV or that they are below the detection limit.

Incident shock velocities are measured close to the sampling orifice by a set of miniature piezoelectric pressure transducers (identified as PT1 to PT4 in Fig. 2(b). The pressure transducers are spaced 76.2 mm apart with PT4 located 27 mm from the end wall of the shock tube. The temperature and pressure behind the reflected shock wave are obtained in a similar manner to the incident shock conditions in the DFST/LS experiments with similar estimated errors in the post

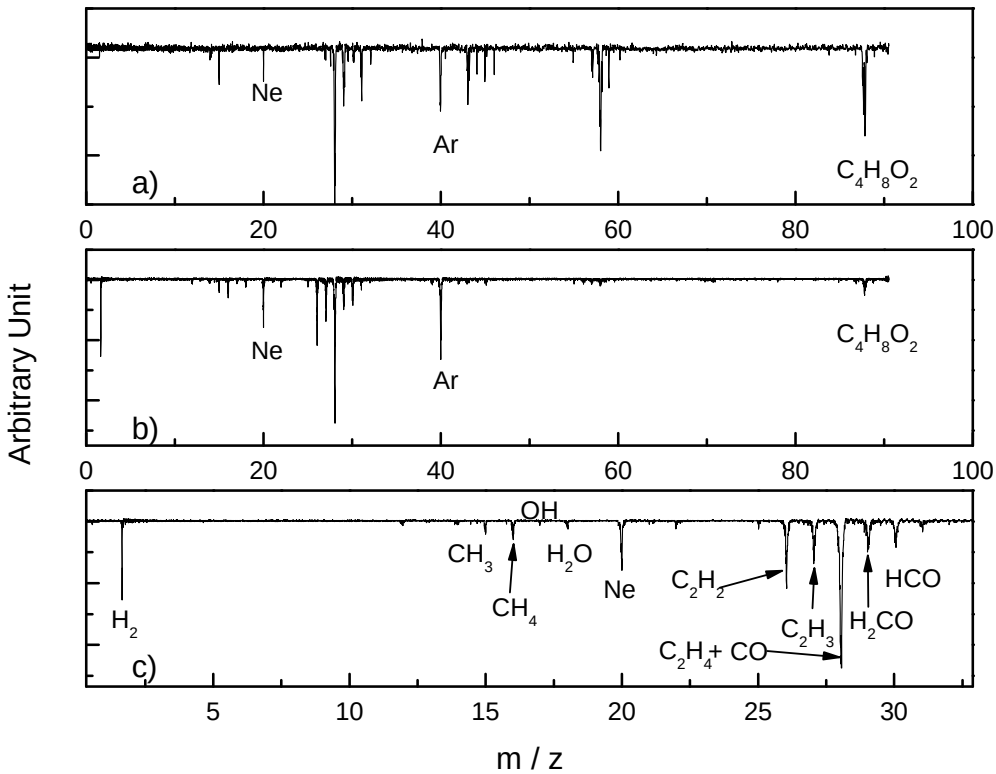


**Figure 4**: Example TOF mass spectra, 30 eV, from the pre- and post shock regions of a DFST/TOF-MS experiments with 4% 1,4-dioxane dilute in neon. Argon was added to the reagent mixture as an internal standard. $T_5$ = 1699 K and $P_5$ = 629 Torr. a) Pre-shock. b) Post-shock, 120 μs after reflection of the incident shock wave. c) expansion of the m/z < 35 region of panel (b).

shock temperature. PT1 is also used to generate a trigger signal for the data acquisition system and initiate generation of ion packets in the TOF-MS.

**Reagent Mixtures:** For the LS experiments mixtures containing 2% 1,4-dioxane dilute in krypton were prepared. While for the DFST/TOF-MS experiments the reagent mixtures contained 4% 1,4-dioxane and 3% argon dilute in neon. All mixtures were prepared manometrically in a 50 L glass vessel that had been evacuated to $<10^{-3}$ Torr. Krypton (AGA 99.999%), was used as supplied. 1,4-Dioxane (Aldrich Chemical Co., 99%) was degassed by repeated freeze–pump–thaw cycles with liquid nitrogen. Reagent mixtures were allowed to homogenize for several hours before use.

## 3. Theory

The potential energy surface associated with the ring opening of 1,4-dioxane was explored using dual level quantum chemistry. Dual level calculations are described using the notation E//G, where E and G denote the methods used to compute the high-level energies and the low-level geometries and frequencies, respectively. We considered both single reference dual level calculations

QCISD(T)/CBS//B3LYP/6-311++G(d,p) and multireference dual level calculations MRCI+Q/CBS//CASPT2/aug-cc-pVDZ. The complete basis set (CBS) limit was estimated using a two point formula [12] and the aug-cc-pVDZ and aug-cc-pVTZ basis sets. In the multireference calculations, the (6e,6o) active space (six electrons in six orbitals) is most appropriate for the multi-bond processes considered here. However, this active space is computationally demanding and the smaller (2e,2o) active space was used in the initial explorations of the potential energy surface presented in this paper. The quantum chemistry calculations were performed using Gaussian [13] and Molpro [14].

**Table I. Zero point inclusive stationary point energies (kcal/mol)**

| Stationary point | $Q_1$[a] | SR[b] | MR[c] | Product |
|---|---|---|---|---|
| 1,4-dioxane ($C_{2h}$) | 0.012 | 0.0 | 0.0 | |
| 1,4-dioxane ($D_2$) | 0.011 | 6.1 | 6.0 | |
| 1,4-dioxane [$C_{2h} \Leftrightarrow D_2$]$^{\ddagger}$ | 0.011 | 10.7 | *d* | |
| SP1-$C_{2h}$ | 0.022 | 78.5 | 87.2 | (C1) $HOCH_2CH_2OCHCH_2$ |
| SP1-$D_2$ | 0.033 | 83.9 | 91.8 | (C1) $HOCH_2CH_2OCHCH_2$ |
| SP2-$C_{2h}$ | 0.103 | *e* | 85.9 | (C2) $CH_3CH_2OCH_2CHO$ |
| SP2-$D_2$ | 0.092 | *e* | 85.0 | (C2) $CH_3CH_2OCH_2CHO$ |
| SP3 | 0.017 | 86.5 | 90.3 | (C3) $CH_3OCH_2CH_2OCH$**:** |
| SP4 | 0.015 | 92.9 | *d* | $CH_2O + C_2H_4 + CH_2O$ |

[a]Q1 diagnostic from the QCISD/aug-cc-pVTZ calculation

[b]Single reference quantum chemistry, QCISD(T)/CBS//B3LYP/6-311++G(d,p)

[c]Multireference quantum chemistry, MRCI+Q/CBS//CASPT2/aug-cc-pVDZ, with the minimal active space (2e,2o)

[d]The (2e,2o) active space is too small to correctly describe this saddle point.

[e]The QCISD(T) calculation failed due to significant multireference character

## 4. Theory Results

The results of the single reference and multireference dual level calculations on the 1,4-dioxane surface are summarized in Table I where the reported stationary point energies include zero point corrections. 1,4-dioxane has two stable conformers: the "chair" (C2h) conformer is lower in energy than the "twist" conformer (D2) by 6 kcal/mol, and the two conformers are separated by a 11 kcal/mol barrier relative to the chair conformer.

Several saddle points associated with the ring opening of both conformers of 1,4-dioxane were identified and are listed in Table I as SPx. Clearly, the energies of all the saddle points are quite similar and with the likely uncertainties in the calculations, discussed below, all of the dissociation pathways are potentially accessible. The saddle points on the 1,4-dioxane potential are analogous to those identified previously in similar multireference calculations for the pyrolysis of cyclohexane [2] where the exclusive decay pathway was determined to be ring opening accompanied by an H atom transfer from the β carbon to the distant C atom involved in the breaking bond to give 1-hexene.

For 1,4-dioxane, the presence of the O heteroatoms results in two distinct processes for scission of a C-O bond that result in different immediate products. Whereas, for cyclohexane the scission of a C-

C bond leads to only one immediate product. The saddle points associated with C-O scission in 1,4-dioxane are identified as SP1 and SP2, where the acceptor atoms in the cross-ring H atom transfer are O and C, respectively. Additionally, saddle points connected to the chair ($C_{2h}$) and twist ($D_2$) forms of 1,4-dioxane are distinct, resulting in four saddle points associated with scission of a C-O bond and these are labeled SP1-$C_{2h}$, SP1-$D_2$, SP2-$C_{2h}$, and SP2-$D_2$, in Table I. The multireference energies of SP1-$C_{2h}$ and SP1-$D_2$, Table I, show a difference of about 4 kcal/mol but both saddle points yield the same immediate product, $HOCH_2CH_2OCHCH_2$ (C1). The difference in MR energies for SP2-$C_{2h}$, and SP2-$D_2$ is < 1 kcal/mol and both saddle points yield $CH_3CH_2OCH_2CHO$ (C2).

SP3 is a ring opening at a C–C bond accompanied by an H-transfer across the opening bond to give $CH_3OCH_2CH_2OCH$ (C3). SP4 is a saddle point for the concerted breaking of 3 bonds, two C–O bonds and one C–C bond, to give 2 $CH_2O$ and $C_2H_4$. SP3 and SP4 are associated only with the chair ($C_{2h}$) form of dioxane, and no distinct saddle points associated with the $D_2$ form of 1,4-dioxane were found for these processes.

As shown in Table I, the QCISD(T) calculations for several of the species discussed above suffer from significant multireference contamination (indicated by $Q_1$ diagnostics greater than ~0.02). In fact, the QCISD(T) single reference method fails entirely for SP2 due to multiference effects.

The multireference dual level approach is in principle more accurate than the single reference approach when $Q_1$ is large, but unfortunately with respect to the 1,4-dioxane potential energy surface the size of the system limits the active space that can be affordably used to compute optimized geometries. However, the MRCI+Q/CBS//B3LYP/6-311++G(d,p) method was tested for a series of active spaces, (2e,2o), (4e,4o), and (6e,6o), for several of the species shown in Table I. The maximum energetic effect due to the active space in these calculations was 4 kcal/mol, with an average effect of less than 1 kcal/mol. The error in the dual level multireference calculations associated with the use of the minimal active space in the geometry optimizations is unknown. For the 1,4-dioxane interconversion saddle point and for SP4, the minimal active space is not able to qualitatively describe the important reference states, and the multiference calculations with the (2e,2o) active space do not provide meaningful results.

Based on the above discussion, it is not clear whether the single reference or multireference approach is more accurate, in general, for the present system. When both methods may be reliably applied to the same species, the difference in their predictions (up to 9 kcal/mol) may be taken as an indication of the uncertainty in either calculation. The range of ring opening saddle point energies reported in Table I is 14 kcal/mol, which is likely close to the uncertainty in the present calculations.

We conclude from these calculations that 1,4-dioxane decomposition may proceed via any of the processes discussed above. Furthermore, the immediate products (C1, C2 and C3) of decomposition via SP1, SP2 and SP3 will undoubtedly lead to a rich secondary chemistry, due to isomerization and decomposition of C1, C2 and C3.

At this stage, the uncertainties in the energetics are too large to warrant conducting a Master Equation analysis to obtain pressure dependant rate coefficients for the different reaction channels. However, the ab-initio calculations do provide a description of potential dissociation paths for 1,4-dioxane. These channels are considered below in the discussion of the simulation of the laser schlieren experimental data, which generally provide a sold test of mechanism. In future work more extensive, computationally intensive, theoretical calculations will be performed guided by the results of the experimental and modeling studies.

## 5. Experimental Results and Discussion

**TOF-MS:** Ten DFST/TOF-MS experiments on the pyrolyis of 1,4-Dioxane dilute in neon were carried out over the temperature range 1400-1800 K and 610 ± 20 Torr. For the example experiment shown in Fig. 4 it is clear that almost all of the 1,4-dioxane has been consumed in the first 120 μs of reaction and the peaks in the post-shock mass spectrum consequently, represent products and not fragments of the parent molecule. In Fig. 4c the product peaks are assigned to $H_2$, $CH_3$, $CH_4$, OH, $H_2O$, $C_2H_2$, $C_2H_3$, $C_2H_4$, CO, HCO and $H_2CO$. Of these species, there are five that are of particular value with respect to understanding the dissociation mechanism of 1,4-dioxane: $CH_3$, $CH_4$, $H_2$, OH and $H_2O$. The m/z for these species cannot be generated by fragmentation of any of the higher mass products ($C_2H_2$, $C_2H_3$, $C_2H_4$, CO, HCO and $H_2CO$), in the ion source and almost all of the 1,4-dioxane has been consumed, thus they can be considered unique products from 1,4-dioxane pyrolysis. The $CH_3$ peak could be a fragment of $CH_4$ and similarly the OH could be a fragment from $H_2O$ however the relative intensities of $CH_3/CH_4$ and $OH/H_2O$ are too large for the lower mass species to be exclusively fragments of the heavier ones.

$CH_4$, $H_2O$ and $H_2$ are likely formed by reactions involving abstraction of H-atoms from other molecules by H, OH and $CH_3$ radicals. Consequently, a mechanism for 1,4-dioxane pyrolysis must generate these species. A potential source of these radicals is $CH_2CHOCH_2CH_2OH$ (C1), the immediate product formed from dissociation of 1,4-dioxane by SP1. C1 can decompose to a vinoxy radical, $CH_2CHO$, and etheneol, $CH_2CH_2OH$. This is followed by dissociation of the vinoxy radical by two routes: H + $CH_2CO$ and $CH_3$ + CO [15]. Etheneol, $CH_2CH_2OH$, dissociates predominantly to OH + $C_2H_4$ [16]. Thus from dissociation of 1,4-dioxane via SP1 a pool of radicals can be developed that are consistent with the TOF-MS results and which will propagate a chain reaction without relying on the thermal dissociation of formaldehyde. This does not preclude dissociation via SP2 or SP3 because the subsequent decomposition of C1 or C3 would generate $CH_3$ and H. However, SP1 is the only direct rout to OH formation indicating it plays some, if not a major role, in dissociation of 1,4-dioxane.

**LS:** Thirty five LS experiments with 1,4-dioxane dilute in krypton were performed at $P_2$ = 123±3 Torr, over the range 1550 < $T_2$ < 2100 K. The first few points of each semi-log density gradient plot in Fig. 3 are due to the end portion of the shock front / laser beam interaction described above. Unfortunately, this masks the location of $t_0$, the time origin at the onset of reaction. Consequently, $t_0$ is located by a well established method [17]. Typically, the time origin is located to an accuracy of 0.1 – 0.2 μs. The initial dissociation rate constant of 1,4-dioxane, $k_1$, is obtained by extrapolation of the density gradient profile back to $t_0$. For the lower temperature and pressure experiments, Fig. 3a, this extrapolation is initially quite accurate, and subsequent refinement of the initial estimate through simulation of the complete density gradient profile typically results in <10% change in $k_1$. The effect on the simulations of varying $k_1$ is demonstratce din Fig. 3a. For the higher temperature experiments determining the density gradient at $t_0$ is more difficult due to the steep slope of the early part of the data and the initial rate coefficients are best determined through simulation of the complete LS profile. However, even in these cases the initial estimates rarely change by more than 10-15%. The initial dissociation rate coefficients for 1,4-dioxane dissociation, reaction (1) in Table II, are shown in Fig. 5 and are represented by the following Arrhenius expression.

$$k_{1,123Torr}(T) = (2.10 \pm 0.30) \times 10^8 \times \exp(-15006/T)\ s^{-1}$$

Given the complexity of the potential energy surface described in theory section and the uncertainties in the calculated energies of the saddle points and species it is not clear whether the measured $k_1$ represent a single channel or a composite from multiple pathways and more detailed theoretical work is required too resolve this point.

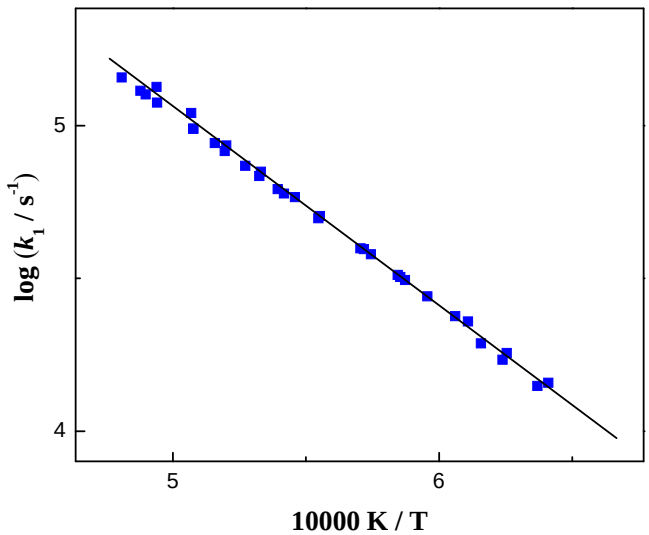


**Figure 5**: First order rate coefficients for the pyrolysis of 1,4-dioxane. Points are the experimental data. The line represents an Arrhenius fit, see text.

**Modeling of LS Experiments:** Simulations of the LS experiments were performed using a computer code designed for reactive flows behind shock waves similar to that outlined in reference [18] which also accounts for temperature changes due to reaction through solution of the energy equation. Reverse reactions were included for all reactions in the mechanism via detailed balance using thermodynamic data from the publication of Burcat and Ruscic [19]. Examples of the simulation results using the mechanism presented in Table II are shown in Fig. 3 and similarly good fits between the simulations and experiments were found over the whole range of experiments. The mechanism in Table II consists of two parts: Reactions (2) – (28) represent a sub-mechanism for the reactions of methyl radicals and was taken from recent LS studies on the dissociation of methyl iodide, and dicaetyl [20,21] over a similar range of temperature and pressure. The remaining reactions, (1) and (29)-(72), are associated with the pyrolysis of 1,4-dioxane, radical attack on the parent and product species, and dissociation of product species. The initial dissociation of 1,4-dioxane and radical attack on 1,4-dioxane are discussed briefly below.
The theoretical studies indicate four potential channels for the dissociation of 1,4-dioxane.

$C_4H_8O_2 \rightarrow HOCH_2CH_2OCHCH_2$ SP1
$\rightarrow CH_3CH_2OCH_2CHO$ SP2
$\rightarrow CH_3OCH_2CH_2OCH$ SP3
$\rightarrow CH_2O + CH_2O + C_2H_4$ SP4

The products of the concerted dissociation of 1,4-dioxane (SP4), $C_2H_4$ and HCHO, are thermally very stable and will not dissociate at the conditions of the current experiments on the time scale of a LS experiment [1]. Consequently, the concerted mechanism cannot promote a chain reaction that would generate $CH_3$, $CH_4$, $H_2$, OH or $H_2O$ which are observed in the post shock mass spectra. Furthermore, SP4 is endothermic by ~36 kcal/mol and cannot, by itself, generate the negative density gradients, characteristic of exothermic reactions, that are found in many of the 1,4-dioxane LS experiments. Thus, it is unlikely that dissociation via SP4 will be a major pathway for pyrolysis of 1,4-dioxane and that the mechanism will be more analogous to that for cyclohexane, bond scission, than for 1,3,5-trioxane which occurs solely by a concerted mechanism. The immediate products, C2 and C3, from dissociation of 1,4-dioxane via SP2 and SP3 could decompose to secondary products that would generate $CH_3$ radicals and H-atoms, as shown above. Previous, LS studies [20,21] have shown that subsequent reactions of $CH_3$ produce strong, negative density gradeints. However, it is not clear that reaction via SP2 or SP3 would lead to the formation of OH radicals and the TOF-MS results clearly indicate the presence of OH and $H_2O$. SP3 is probably not a significant channel due to the diradical character of C3. Reaction via SP2 however is likely competitive with dissociation via SP1 which through the subsequent decomposition of vinoxy and etheneol gives $CH_3$, H and OH. Consequently, either reaction via SP1 alone or more likely some combination of SP1 and SP2 can satisfy the requirements imposed by both the TOF-MS and LS experimental data. A simplified potential energy surface for dissociation by SP1 and SP2 and the initial dissociation of their products is given in Fig. 6.

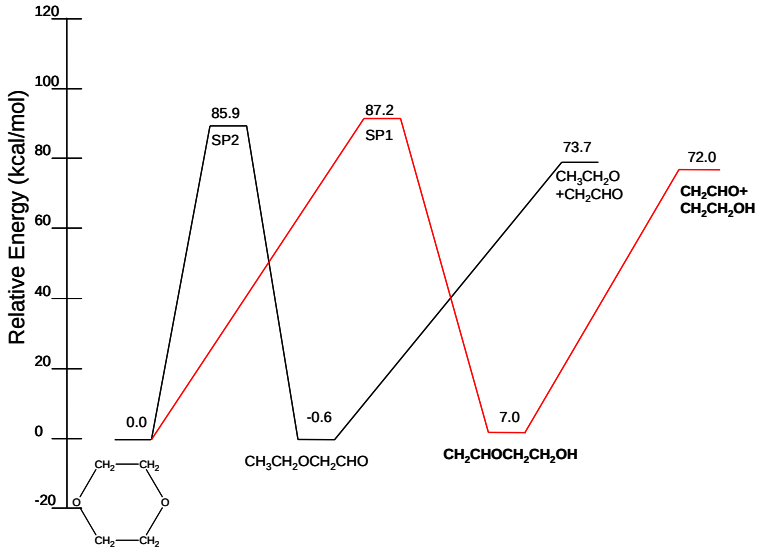


**Figure 6:** Simplified potential energy surface for the decomposition of $C_4H_8O_2$ . Energies are in kcal/mol and were computed at the G3B3 level with the exception of SP1 and SP2 which are MR energies from Table I. The red line represents reaction (1) in Table (II).

A large number of simulations have been performed to test various hypotheses regarding the dissociation of 1,4-dioxane. The simulations presented here are based on a mechanism, Table II, that incorporates SP1 as the only dissociation pathway for 1,4-dioxane and these simulations give very good predictions of the experimental density gradients, Fig. 3. Reaction (1) also assumes immediate dissociation of C1 to vinoxy and etheneol. It is recognized that is probably an oversimplification and it maybe that C1 is in fact stabilized and then subsequently reacts. Additional experimental studies are being conducted to study the dissociation of C1 directly by LS to address this point. Furthermore,

it is most likely that SP2 plays some role in the dissociation of 1,4-dioxane and even higher level theoretical investigations of SP1 and SP2 are being conducted to assess their relative contributions.
The dissociation of vinoxy, reactions (29) and (30) and ethenol, reaction (35), generates H, OH and $CH_3$ which can abstract an H-atom from 1,4-dioxane by reactions (36), (37) and (70) respectively, to form the radical $C_4H_7O_2$. Reaction (37), OH + 1,4-dioxane, has been studied by Moriarty et al. [22], Maurer et al[23] and Porter et al. [24] at 298 K. Their results are in good agreement and provided an initial estimate for $k_{37}$. Rate coefficients for reactions (36), H + $C_4H_8O_2$, and (70), $CH_3$ +$C_4H_8O_2$, were estimated from H + oxirane [25] and $CH_3$ + oxirane [26] respectively. Both of these reactions are nearly thermoneutral, $\Delta H_{r,298}$ ~ -0.8 kcal/mol, and therefore contribute little to the density gradient. Thus they were not adjusted beyond the values given in Table II. The simulations of the density gradient profiles were quite sensitive to the value of $k_{37}$, Fig. 3b, and this parameter was optimized for each experiment. The bimolecular rate coefficients determined for $k_{37}$ were fitted by a non-Arrhenius expression, given below, which is valid over the range 1500 – 2100 K, and is in reasonable agreement with the low temperature determination of $k_{37}$ by Moriarty et al.

$$k_{37} = (2.25 \pm 0.60) \times 10^3 \times T^3 \times \exp(860/T)\ \mathrm{cm^3 mol^{-1} s^{-1}}$$

With the mechanism in Table II the primary sources of negative density gradients at all reaction temperatures are reactions (37), (40, H + HCO → $H_2$ +CO), (45, $CH_3$ + HCO → $CH_4$ + CO) and (50, OH + HCO → $H_2O$ + CO) all of which are roughly 90 kcal/mol exothermic. The self reaction of methyl radicals makes almost no contribution to the calculated density gradient as the methyl radicals are primarily consumed by reaction (45).
The chain reaction in the dissociation of 1,4-dioxane is initiated by the formation of $C_4H_7O_2$ and the subsequent decomposition of this radical via reaction (38). There are no literature data concerning the dissociation of $C_4H_7O_2$. Consequently, the decomposition pathways have been explored, preliminarily, by ab-initio calculations using the G3B3 method and the potential energy surface is shown in Fig. 7. The lowest energy pathway generates $C_2H_4$, HCHO and HCO. The subsequent fast decomposition of HCO to H + CO [28] propagates the chain reaction.

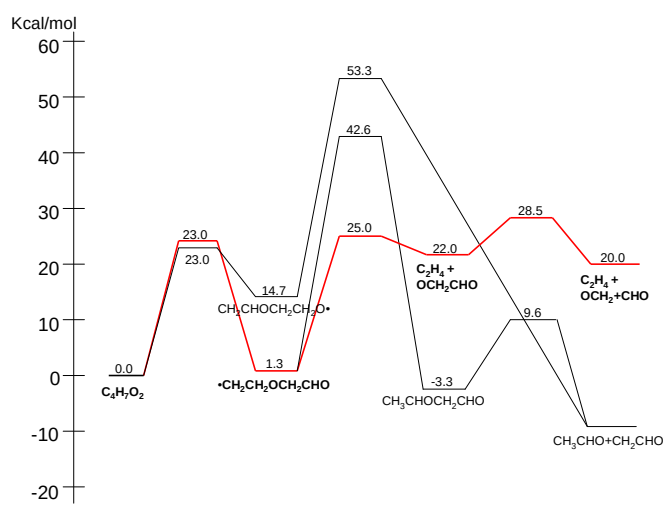


b)

**Figure 7:** Schematic potential energy surface for the decomposition of $C_4H_7O_2$ . Energies are in kcal/mol and were computed at the G3B3 level. The red line indicates the lowest energy path.

## Concluding Remarks

A detailed, although still somewhat preliminary, investigation of the pyrolysis of 1,4-dioxane has been conducted using complementary experimental and theoretical methods. It has been demonstrated that the dissociation does not occur via a concerted reaction but rather by ring opening and dissociation of the resulting linear species generates H, OH and $CH_3$ radicals that propagate a chain mechanism. The initial modeling results indicate that the LS profiles can be satisfactorily simulated with the mechanism in Table II that assumes dissociation of 1,4-dioxane by only SP1. However, this is likely an oversimplification and neglects the potential contribution from SP2. Additional, experimental and theoretical work is being conducted to try and assess the contributions from alternative dissociation channels for the initial dissociation of 1,4-dioxane.

## Acknowledgments

This work was performed under the auspices of the Office of Basic Energy Sciences, Division of Chemical Sciences, Geosciences, and Biosciences, U.S. Department of Energy, under contract numbers DE-AC02-06CH11357, DE-AC04-94-AL85000, DE-FE-85ER13384.

## References

[1] E. A. Irdam, J. H. Kiefer, *Chemical Physics Letters*, 166 (1990), 491-494; V. Vasudevan, D. F. Davidson, R. K. Hanson, C. T. Bowman, D. M. Golden, *Proceeding of the Combustion Institute*, 31 (2007) 175-183.

[2] Gupte, K. S. Doctoral Thesis, University of Illinois at Chicago, 2009. K. S. Gupte, J. H. Kiefer, L. B. Harding, unpublished work, 2009.

[3] L. Kuchler, J. D. Lambert, *Zeitschrift für Physikalische Chemie*, B37 (1936), 285.

[4] F. Battin, P. M. Marquaire, F. Baronnet, G. M. Come, *Journal of Analytical and Applied Pyrolysis* 16 (1989) 345-354.

[5] E. A. Irdam, J. H. Kiefer, L. B. Harding, A. F. Wagner, *International Journal of Chemical Kinetics* 25 (1993) 285-303; S. S. Kumaran, U. J. Carroll, J. V. Michael *Proceeding of the Combustion Symposium,* 27 (1998) 125-133

[6] R. S. Tranter and B .R. Giri, *Review of Scientific Instruments*, 79 (2008) 0941031.

[7] J. H. Kiefer and A. C. Manson, *Review of Scientific Instruments,* 52 (1981) 1392-1396.

[8] J. H. Kiefer, in A. Lifshitz (Ed.), *Shock Waves in Chemistry* Marcel Dekker, New York, 1981, pp. 219-277.

[9] W. C. Gardiner, Y. Hidaka and T. Tanzawa, C*ombustion and Flame* 40 (1981) 213-219.

[10] B. R. Giri, R. S. Tranter, *Review of Scientific Instruments,* 78 (2007 034101

[11] NIST Mass Spec Data Center, S.E. Stein, director, " Mass Spectra " in NIST Chemistry WebBook, NIST Standard Reference Database Number 69, Eds. P.J. Linstrom and W.G. Mallard, June 2005, National Institute of Standards and Technology, Gaithersburg MD, 20899 (http://webbook.nist.gov).

[12] J. M. L. Martin, O. Uzan, *Chemical Physics Letters*, 282(1998), 16-24.

[13] Gaussian 98, Revision A.7, M. J. Frisch, G. W. Trucks, H. B. Schlegel, G. E. Scuseria, M. A. Robb, J. R. Cheeseman, Jr., J. A. Montgomery, T. Vreven, K. N. Kudin, J. C. Burant, J. M. Millam, S. S. Iyengar, J. Tomasi, V. Barone, B. Mennucci, M. Cossi, G. Scalmani, N. Rega, G. A. Petersson, H. Nakatsuji, M. Hada, M. Ehara, K. Toyota, R. Fukuda, J. Hasegawa, M. Ishida, T. Nakajima, Y. Honda, O. Kitao, H. Nakai, M. Klene, X. Li, J. E. Knox, H. P. Hratchian, J. B. Cross, V. Bakken, C. Adamo, J. Jaramillo, R. Gomperts, R. E. Stratmann, O. Yazyev, A. J. Austin, R. Cammi, C. Pomelli, J. W. Ochterski, P. Y. Ayala, K. Morokuma, G. A. Voth, P. Salvador, J. J. Dannenberg, V. G. Zakrzewski, S. Dapprich, A. D. Daniels, M. C. Strain, O. Farkas, D. K. Malick, A. D. Rabuck, K. Raghavachari, J. B. Foresman, J. V. Ortiz, Q. Cui, A. G. Baboul, S. Clifford, J. Cioslowski, B. B. Stefanov, G. Liu, A. Liashenko, P. Piskorz, I. Komaromi, R. L. Martin, D. J. Fox, T. Keith, M. A. Al-Laham, C. Y. Peng, A. Nanayakkara, M. Challacombe, P. M. W. Gill, B. Johnson, W. Chen, M. W. Wong, C. Gonzalez, J. A. Pople, Gaussian, Inc., Wallingford CT, 2004

[14] MOLPRO, Version 2006.1, H.-J. Werner, P. J. Knowles, R. Lindh, F. R. Manby, M. Schütz, P. Celani, T. Korona, G. Rauhut, R. D. Amos, A. Bernhardsson, A. Berning, D. L. Cooper, M. J. O. Deegan, A. J. Dobbyn, F. Eckert, C. Hampel, G. Hetzer, A. W. Lloyd, S. J. McNicholas, W. Meyer, M. E. Mura, A. Nicklaß, P. Palmieri, R. Pitzer, U. Schumann, H. Stoll, A. R. J. Stone Tarroni, T. Thorsteinsson.

[15] J. P. Senosiain, S. J. Klippenstein, J. A. Miller, *Journal of Physical Chemistry A*, 110(2006), 5772-5781.

[16] R.S. Zhu, J. Park, M.C. Lin, *Chemical Physics Letters*, 408 (2005) 25-30

[17] J. H. Kiefer, M. Z. Al-alami, J. C. Hajduk, *Applied Optics*, 20 (1981) 221-230.

[18] W. C. Gardiner, B. F. Walker, C. B.Wakefield, in: A. Lifshitz (Ed.), *Shock Waves in Chemistry* Marcel Dekker inc, New York, 1981, pp. 319-374.

[19] A. Burcat, B. Ruscic, Ideal Gas Thermochemical Database with updates from Active Thermochemical Tables,ftp://ftp.technion.ac.il/pub/supported/aetdd/thermodynamics
[20] X. L. Yang, C. F. Goldsmith, R. S. Tranter, *Journal of Physical Chemistry A*, 113 (2009) 8307-8317
[21] X. L. Yang, A. W. Jasper, J. H. Kiefer, R. S. Tranter, *Journal of Physical Chemistry A*, 113 (2009) 8318-8326
[22] J. Moriarty, H. Sidebottom, J. Wenger, A. Mellouki, G. Le Bras, *Journal of Physical Chemistry A*, 107(2003) 1499-1505
[23] T. Maurer, H. Hass, I. Barnes, K. H. Becker, *Journal of Physical Chemistry A*, 103 (1999) 5032-5039
[24] E. Porter, J. Wenger, J. Treacy, H. Sidebottom, A. Mellouki, S. Teton, G. LeBras, *Journal of Physical Chemistry A*, 101 (1997) 5770-5775
[25] A. Lifshitz, H. Ben-Hamou, *Journal of Physical Chemistry*, 87(1983) 1782-1787
[26] R. R. Baldwin, A. Keen, R.W. Walker *Journal of Chemical Society Faraday Transaction.* 80(1984)435-456
[27] G. P. Smith, D. M. Golden, M. Frenklach, N. W. Moriarty, B. Eiteneer, M. Goldenberg, C. T. Bowman, R. K. Hanson, S. Song, W. C. Gardiner, V V. Lissianski, Z. W. Qin, `http://www.me.berkeley.edu/gri_mech`
[28] G. Friedrichs, J. T. Herbon, D.F. Davidson, R.K. Hanson, *Physical Chemistry Chemical Physics* 4 (2002)5778-5788
[29] J. Troe, *Journal of Physical Chemistry A*, 111 (2007) 3862-3867
[30] D. L. Baulch, C. T. Bowman, C. J. Cobos, R .A. Cox, T. Just, J. A. Kerr, M. J. Pilling, D. Stocker, J. Troe, W. Tsang, R. W. Walker and J. Warnatz, *Journal of Physical and Chemical Reference Data*, 34 (2005) 757-1397.
[31] D. L. Baulch, C. J. Cobos, R .A. Cox, C. Esser, P. Frank,; Th. Just, J. A. Kerr, M. J. Pilling, Troe, J. R.W. Walker, J. Warnatz, *Journal of Physical and Chemical Reference Data*, 21 (1992) 411
[32] V. Vasudevan, D. F. Davidson, R.K. Hanson, *International Journal of Chemical Kinetics*, 37 (2005) 98-109
[33] N.K. Srinivasan, M.C. Su, J.W.Sutherland, J.V. Michael, *Journal of Physical Chemistry A*, 109 (2005) 1857-1863
[34] N.K. Srinivasan, M.C. Su, J.V. Michael, *Physical Chemistry Chemical Physics*, 9 (2007) 4155-4163
[35] A.W. Jasper, S. J. Klippenstein, L. B. Harding, B. Ruscic, *Journal of Physical Chemistry A*, 111 (2007) 3932-3950
[36] N.K. Srinivasan, M.C. Su, J.V. Michael, *Journal of Physical Chemistry A*, 111 (2007) 3951-3958
[37] S.R. Sellevag, Y. Georgievskii, J.A Miller, *Journal of Physical Chemistry A*, 112 (2008) 5085-5095
[38] W. Tsang *Journal of Physical and Chemical Reference Data*, 16 (1987) 471-
[39] A. E. Lutz, R. J. Kee, J. A. Miller, H. A. Dwyer, A. K. Oppenheim, *22nd Symposium (International) on Combustion*, (1989) pp 1683.
[40] Senosiain, J. P.; Klippenstein, S. J.; Miller, J. A. *Journal of Physical Chemistry A*, 109 (2005), 6045-6055.
[41] L.N. Krasnoperov, J.V. Michael, *Journal of Physical Chemistry A*, 108 (2004) 5643 - 5648
[42] Woods T.; Haynes B.S. *Twenty-Fifth Symposium (International) on Combustion*, The Combustion Institute, Pittsburgh, Pa. 1994, pp 909-917.
[43] S. I. Stoliarov, V.D. Knyazev, I. R. Slagle, *Journal of Physical Chemistry A*, 104 (2000) 9687 - 9697

**Table II: Reaction mechanism and Arrhenius parameters for 1,4-Dioxane pyrolysis at 123 Torr.**

| | Reaction | logA | n | E(kcal/mol) | $\Delta H_{r,298}$ | Source |
|---|---|---|---|---|---|---|
| 1 | $C_4H_8O_2 = CH_2CH_2OH + CH_2CHO$ | 8.344 | 0.00 | 30.000 | 71.03 | This work |
| 2-28 | $C_2H_6 + M = CH_3 + CH_3 + M$ | 64.945 | -12.78 | 111.67 | 90.16 | a |
| 29 | $CH_2CHO + M = CH_3 + CO + M$ | 32.804 | -6.57 | 44.288 | -5.59 | 20 |
| 30 | $CH_2CHO + M = CH_2CO + H + M$ | 30.275 | -5.86 | 46.120 | 37.45 | 20 |
| 31 | $CH_2CO + H = CH_3 + CO$ | 8.890 | 1.45 | 2.840 | -61.85 | 20 |
| 32 | $H + CH_2CHO = CH_3 + HCO$ | 13.300 | 0.00 | 0.000 | -9.98 | 27 |
| 33 | $H + CH_2CHO = CH_2CO + H_2$ | 13.000 | 0.00 | 0.000 | -66.76 | 27 |
| 34 | $CH_3 + CH_2CHO = CH_4 + CH_2CO$ | 12.000 | -0.00 | 0.000 | 67.60 | estimated |
| 35 | $C_2H_4 + OH = CH_2CH_2OH$ | 14.700 | 0.00 | 2.470 | -28.75 | estimated |
| 36 | $H + C_4H_8O_2 = H_2 + C_4H_7O_2$ | 13.000 | 0.00 | 8.500 | -5.95 | estimated |
| 37 | $OH + C_4H_8O_2 = C_4H_7O_2 + H_2O$ | 3.350 | 3.00 | -1.710 | -20.61 | This work |
| 38 | $C_4H_7O_2 = HCO + CH_2O + C_2H_4$ | 14.000 | -1.00 | 35.000 | 25.78 | estimated |
| 39 | $HCO + M = H + CO + M$ | 13.600 | 0.00 | 15.530 | 15.58 | 28 |
| 40 | $H + HCO = H_2 + CO$ | 14.000 | 0.00 | 0.000 | -88.63 | 28 |
| 41 | $H + H_2CO = H_2 + HCO$ | 7.759 | 1.90 | 2.749 | -16.08 | 28 |
| 42 | $HCO + HCO = CH_2O + CO$ | 13.431 | 0.00 | 0.000 | -72.59 | 28 |
| 43 | $CH_2O + M = H + HCO$ | 36.100 | -5.50 | 93.929 | 88.16 | 29 |
| 44 | $CH_2O + M = H_2 + CO$ | 38.640 | -6.10 | 93.929 | -0.46 | 29 |
| 45 | $CH_3 + HCO = CH_4 + CO$ | 13.423 | 0.00 | 0.000 | -89.47 | 27 |
| 46 | $CH_3 + CH_2O = HCO + CH_4$ | 1.500 | 3.36 | 4.310 | -16.88 | 30 |
| 47 | $OH + CH_2CHO = CH_2CO + H_2O$ | 13.100 | 0.00 | 0.000 | -81.42 | 27 |
| 48 | $OH + CH_2CO = CH_2OH + CO$ | 12.225 | 0.00 | -1.010 | -27.83 | 31 |
| 49 | $OH + CH_2O = HCO + H_2O$ | 7.893 | 1.63 | -1.055 | -30.70 | 32 |
| 50 | $OH + HCO = H_2O + CO$ | 13.700 | 0.00 | 0.000 | -103.29 | 31 |
| 51 | $OH + CO = H + CO_2$ | 6.800 | 1.50 | -0.500 | -21.68 | 31 |
| 52 | $OH + CH_4 = CH_3 + H_2O$ | 13.757 | 0.00 | 8.215 | -13.82 | 33 |
| 53 | $OH + C_2H_4 = C_2H_3 + H_2O$ | -0.880 | 4.20 | -0.860 | -7.88 | 34 |
| 54 | $OH + CH_3 = CH_2(T) + H_2O$ | 4.620 | 2.57 | 4.000 | -8.32 | 35 |
| 55 | $OH + CH_3 = CH_2(S) + H_2O$ | 11.220 | 0.30 | 12.547 | 0.66 | 35 |
| 56 | $OH + CH_3 = CH_2OH + H$ | 9.782 | 1.00 | 3.191 | 4.02 | 35 |
| 57 | $OH + CH_3 = HCOH + H_2$ | -11.08 | 6.41 | -2.483 | -13.82 | 35 |
| 58 | $CH_3OH = CH_3 + OH$ | 15.748 | 0.00 | 61.600 | 92.05 | 36 |
| 59 | $OH + H + M = H_2O + M$ | 20.500 | -1.53 | 0.370 | -118.86 | 37 |
| 60 | $CH_2OH + M = CH_2O + H + M$ | 43.100 | -8.00 | 43.000 | 30.21 | 38 |
| 61 | $HCOH = CH_2O$ | 13.640 | 0.00 | 30.110 | 55.97 | estimated |
| 62 | $OH + C_2H_3 = C2H_2 + H_2O$ | 12.700 | 0.00 | 0.000 | -83.84 | 39 |
| 63 | $OH + C_2H_2 = CH_2CO + H$ | 5.500 | 1.92 | 0.600 | -22.57 | 40 |
| 64 | $OH + C_2H_2 = CH_3 + CO$ | 7.880 | 1.05 | 1.111 | -54.67 | 40 |
| 65 | $OH + H_2 = H_2O + H$ | 8.320 | 1.52 | 3.430 | -14.66 | 41 |
| 66 | $OH + C_2H_6 = C_2H_5 + H_2O$ | 13.820 | 0.00 | 5.040 | -18.11 | 41 |
| 67 | $CH_3 + CH_2CO = C_2H_5 + CO$ | 11.000 | 0.00 | 0.000 | -21.26 | 42 |
| 68 | $CH_3 + C_2H_3 = C_2H_2 + CH_4$ | 11.500 | 0.00 | 0.000 | -69.84 | 43 |
| 69 | $CH_3 + C_2H_4 = C_2H_3 + CH_4$ | 12.617 | 0.00 | 11.128 | 5.94 | 31 |
| 70 | $CH_3 + C_4H_8O_2 = C_4H_7O_2 + CH_4$ | 12.300 | -0.00 | 12.000 | -6.79 | estimated |
| 71 | $OH + OH = H_2O + O$ | 4.553 | 2.42 | -2.110 | -16.17 | 27 |
| 72 | $O + C_4H8O_2 = OH + C_4H_7O_2$ | 13.050 | 0.00 | 0.000 | -4.44 | estimated |

Units: kcal/mol, mole, $cm^3$, s. the values shown for reactions 1 and 37, highlighted in red, have been optimized for 123 Torr. a) sub-mechanism for recombination of methyl radicals from references [19,25,26].